Geoarchaeology

WILEY

Geoarchaeology An International Journal

RESEARCH ARTICLE OPEN ACCESS

Late Holocene Evolution of the Lagoonal Harbour of the Punic Centre of Othoca (Western Sardinia, Mediterranean Sea)

Giovanni De Falco[1] | Alfredo Carannante[2] | Carla Del Vais[3] | Luca Gasperini[4] | Ignazio Sanna[5] | Fabio Cammarano[6] | Marilena Cozzolino[7] | Vincenzo Pascucci[8] | Alessandro Conforti[1]

[1]CNR-IAS, Istituto per lo studio degli Impatti Antropici e Sostenibilità in ambiente marino, Sede Secondaria Oristano, Località Sa Mardini, Oristano, Italy | [2]International Research Institute for Archaeology and Ethnology, Napoli, Italy | [3]Università degli Studi di Cagliari, Dipartimento di Lettere, Lingue e Beni Culturali, Cittadella dei Musei, Cagliari, Italy | [4]CNR-ISMAR, Istituto di Scienze Marine, Sede Secondaria Bologna, Bologna, Italy | [5]Soprintendenza ABAP per la città metropolitana di Cagliari e le province di Oristano e Sud Sardegna, Cagliari, Italy | [6]Dipartimento di Scienze, Università degli Studi di Roma Tre, Roma, Italy | [7]Department of Agriculture, Environment and Food, Via De Sanctis Snc, Università degli Studi del Molise, Campobasso, Italy | [8]DADU-Dipartimento di Architettura, Design e Urbanistica Palazzo del Pou Salit, Università degli Studi di Sassari, Sassari, Italy

Correspondence: Giovanni De Falco (giovanni.defalco@cnr.it)

Received: 2 March 2025 | **Revised:** 2 March 2025 | **Accepted:** 28 March 2025

Scientific Editor: Morhange Christophe

Funding: The work has been funded by grant Legge Regionale 7/2007 Project: "Interazioni tra uomo e ambiente nell'evoluzione del paesaggio costiero antico della Sardegna," funded by Regione Autonoma della Sardegna (RAS), Assessorato della Programmazione, Bilancio, Credito e Assetto del Territorio (Base Research Project, L.R. 7 agosto 2007, n. 7, Annualità 2013 (Resp. Carla Del Vais). Partial funding was provided by the projects RITMARE ICM Golfo di Oristano—Linea Dati (Reso. Giovanni De Falco), funded by the Italian Ministry of Research and Education and DESIRMED Demonstration and mainstreaming of Nature-based Solutions for Climate Resilient transformation in the Mediterranean, under the call HORIZON-MISS-2022-CLIMA-01-06, Grant Agreement No 101112972.

Keywords: geophysics | lagoon | Punic | river | sediment core

ABSTRACT

Geophysical surveys and multiproxy analyses of sediment cores have been used to reconstruct the palaeoenvironmental evolution of the Santa Giusta coastal lagoon (SGL), along the western coast of Sardinia. This area served as a natural harbour mainly during the Punic and Roman Republican periods (6th–2nd century BC). The inlet of the SGL is connected to the adjacent mouth of the River Tirso and lies on the incised valley of an ancient tributary that once fed into the Tirso during the last sea-level lowstand. The SGL formed after the sea level rose following the LGM, resulting in the inundation of the incised valleys, which were subsequently filled with estuarine sediments. About 6000 years ago, the area that is now occupied by the mouth of the river and the SGL was protected by a sandy barrier enclosing an open lagoon. About 4500 years ago, the deposition of alluvial sediments marked the beginning of the progradation of the river mouth, leading to the gradual enclosure of the SGL. Before 2100 years ago, the SGL was a suitable location for a sheltered harbour, as evidenced by archaeological indicators, both pottery and wooden structures, found within the lagoon sediments. By this time, the progressive narrowing of the inlet had reduced the accessibility of the site from the sea and the harbour lost its functionality.

1 | Introduction

Coastal lagoons have been attractive locations for human settlements and are used as harbours since ancient times, as they constitute naturally sheltered areas (Kaniewski et al. 2018; Morhange et al. 2017; Marriner and Morhange 2007). Coastal lagoons are often associated with river deltas and the evolution of these complex systems controls their formation, development and eventual filling with sediment (Ruiz-Pérez and Carmona 2019). As far as the deltaic systems of Mediterranean rivers are concerned, two main evolutionary phases have been recognised during the Holocene. These are related to the rate of sea-level rise, climatic variations, sediment input and human impact (Anthony et al. 2014). The first phase is associated with the progradation of clastic coasts after the sea level stabilised, since about 6 ka (Giaime et al. 2022; Giaime et al. 2019; Anthony et al. 2014; Catuneanu and Zecchin 2013). The second phase involves the expansion of deltaic depositional systems and the formation of sand spits and beaches, which are the direct consequence of the increase in sediment input due to the impact of human societies (Maselli and Trincardi 2013; Bellotti et al. 2011). During the evolution of river deltas, coastal lagoons could form and remain isolated from the sea by the development of sand barriers, before being partially or completely filled by sediments. The lagoons that border the Mediterranean coasts to date cover approximately 64,000 km^2 (Cataudella et al. 2015), but were probably wider in ancient times, before being partially filled by sediments (Giaime et al. 2019 and references therein). Due to sediment deposition, several Mediterranean lagoonal harbours lost their function over time and were gradually abandoned. A few examples are the Portus Pisanus, Tuscany (Italy), which was used as a harbour from the 2nd century BC until almost AD ~1500 (Kaniewski et al. 2018); the lagoon of Cumae-Licola (Campania, Italy), which has undergone rapid filling since the Hellenistic period (Stefaniuk and Morhange 2010); and the ancient lagoon of Pollentia (Mallorca, Spain), which has been dredged since its foundation in the 1st century BC (Giaime et al. 2017).

The position of the Sardinia Island, in the centre of the western Mediterranean Sea, has always been attractive, and this is the reason why numerous archaeological settlements have been found along its coasts, especially from the Neolithic (e.g., IIPP 2009) to Late Antiquity. Three important settlements, Tharros, Othoca and Neapolis, founded by the Western Phoenicians, are located along the coast of the Gulf of Oristano, a wide bay on the mid-western coast of Sardinia (Del Vais et al. 2023a, 2023b, 2020; Del Vais 2014; Spanu and Zucca 2011; Del Vais et al. 2008; Acquaro et al. 1999). The city of Othoca, built to control the central sector of the Gulf of Oristano and its rich hinterland (Del Vais 2018, 2010), is located on the northeastern shore of the Santa Giusta lagoon (SGL), a wide coastal lagoon associated with the delta of the Tirso River, the longest river in Sardinia (Figure 1). Underwater excavations in the lagoon have revealed the presence of exceptionally important archaeological remains mainly of the Punic and Roman Republican age (Del Vais et al. 2023a; Del Vais and Sanna 2012). Indeed, pottery mainly dating from the 6th to 2nd centuries BC was recovered buried in the sediments of the SGL, mostly represented by transport amphorae, but also including domestic pottery and, more rarely, pottery associated with funerary and cultic use, in addition to a large amount of organic material (Del Vais et al. 2023a; Del Vais and Sanna 2012). To understand how the geomorphological evolution of the surrounding area has influenced the presence and development of the human settlements, it is an important task to reconstruct the palaeoenvironmental evolution of the lagoon.

The aim of this study is to reconstruct the morpho-stratigraphic evolution of the SGL and the adjacent alluvial plain of the River Tirso over the last 7000 years, with a specific focus on the phases of flooding and progradation of the alluvial system and to relate it with the human occupation of the lagoon since Archaic Punic times (7th–6th century BC).

2 | Study Area

2.1 | Geological Setting and Coastal Geomorphology

The study area (Figure 1) is located in the northern sector of the Campidano Plain, a Pliocene-Quaternary NW-SE-oriented graben, filled by syn-rift continental deposits interspersed with Pliocene basaltic lava flows (Casula et al. 2001). Although a recent study suggests continuous tectonic activity since the Marine Isotopic Stage 7 (MIS7; ca. 220 ka) (Cocco et al. 2019), the basin is generally considered stable since the Middle Pleistocene (post 700 ka) (Cherchi et al. 2008). The northern sector of the Campidano plain overlooks the Gulf of Oristano, a wide and shallow bay protected by two rocky promontories (Figure 1).

The geological setting of the coastal plain includes terraced coarse deposits of Pleistocene age in the inner sector and littoral, alluvial and lagoonal deposits of Holocene age along the coastal sector and the alluvial plain (Figure 1).

The northern side of the Campidano plain is drained by the 150 km long River Tirso and includes several coastal lagoons (Figure 1). The river forms a delta system that flows into the Gulf of Oristano and has a catchment area of about 3340 km^2. It crosses a hilly area until about 20 km from the mouth, where a knickpoint characterises the entrance of the river into the alluvial plain.

The present geomorphological setting of the area is the result of a progressive filling of the incised valley of the River Tirso and of the subsequent formation of coastal barriers and sand spits that close the coastal lagoons (De Falco et al. 2022; Pascucci et al. 2018; Melis et al. 2017).

The infill of the incised valley was characterised by high sedimentation rates associated with the humid period of 8–7 ka BP and lower rates associated with the dry period of the cold phase of 6–4 ka BP (De Falco et al. 2022). The decrease in the rate of sea-level rise after 6 ka allowed for the formation of coastal systems (De Falco et al. 2022; Pascucci et al. 2018; Melis et al. 2017). After 4.5 ka BP, coarse-grained alluvial sediments were deposited because of river mouth progradation (De Falco et al. 2022; Melis et al. 2017).

The SGL (surface area 0.8 km^2, mean depth 1 m) is located south of the alluvial plain of the River Tirso and is connected to

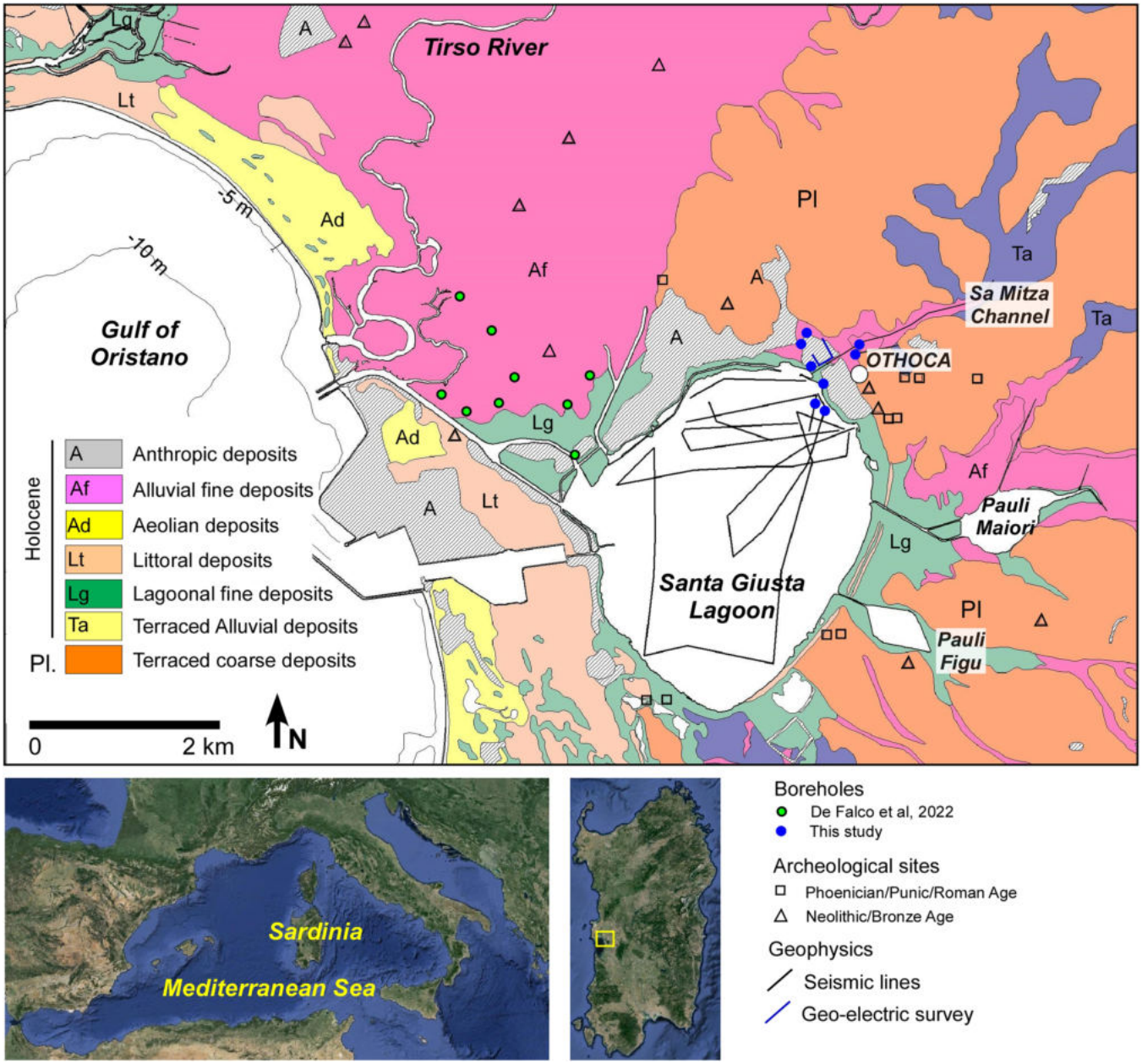

FIGURE 1 | Geological map of the Tirso River mouth and the Santa Giusta lagoon coastal area. The map shows the position of sediment cores collected for this study (blue dots) and the position of the sediment cores described by De Falco et al. (2022) collected along the alluvial plane of River Tirso. The triangle and square symbols indicate the position of archaeological remains along the coastal area. The routes of the seismic lines collected inside the lagoon and position of geo-electric survey lines are also reported.

the sea by an artificial narrow inlet (Pesaria channel, Figure 1). Until recently, the lagoon was connected to the last stretch of the River Tirso by a sinuous inlet, as can be seen in the geographical maps from the 1800s. After 1954, the inlet was straightened and connected directly to the sea. On the eastern shore, three small freshwater tributaries flow into the lagoon (Figure 1). The water inflow is currently mainly regulated by artificial channels.

2.2 | Human Settlements

The central western Sardinia was intensely occupied since the Neolithic, and numerous human settlements from the prehistoric, protohistoric, Punic, Roman and medieval periods were found in this area. In the Oristano area, ancient human settlements were mainly located along the lagoon shores and in the inner sector of the alluvial plain (Figure 2), whereas settlements in proximity of the river mouth are very rare; of the latter, the temporary village of Sa Osa, occupied in the Chalcolithic and especially in the Bronze Age, is the one best documented by archaeological excavations (Usai et al. 2012; Melis et al. 2017).

The Punic centre of Othoca, founded at least in the 7th century BC, is located along the north-eastern shore of the SGL (Figure 2), on a slightly raised alluvial terrace, south of the Sa Mitza channel, one of the freshwater tributaries of the lagoon. The remains of the ancient city lie below the modern village

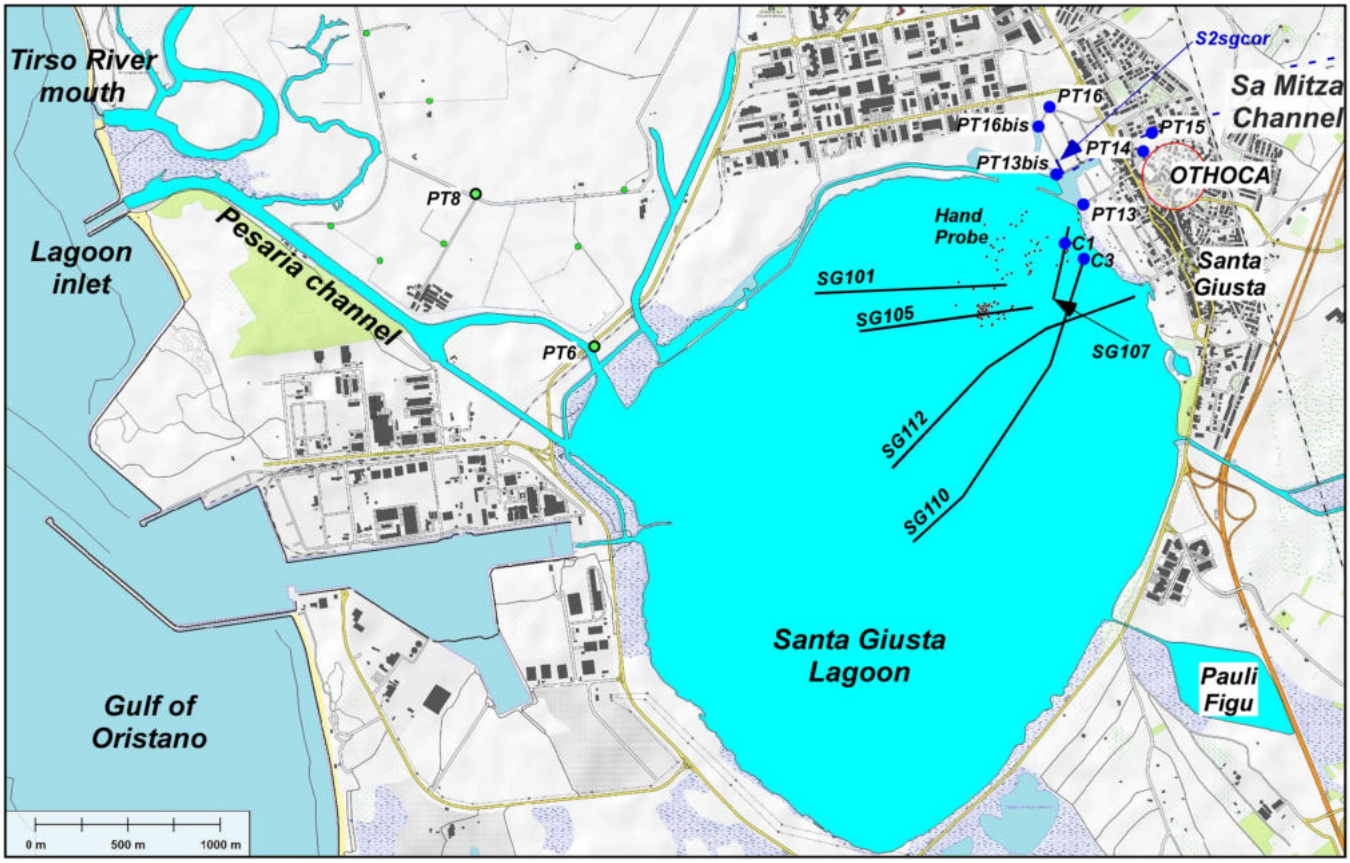

FIGURE 2 | The map shows the routes of seismic lines reported in Figures 2 and 4, the position of sediment cores described in Figures 6 and 7 and the position of the resistivity tomography section reported in Figure 5. The sediment cores PT6 and PT8, described by De Falco et al. (2022), were included in the stratigraphic correlation reported in Figure 9. The dots inside the lagoon show the position of archaeological remains identified inside the lagoon sediments by hand probe surveys (Del Vais and Sanna 2012).

of Santa Giusta; only a few residential contexts and two burial areas from the Punic-Roman period (7th century BC–1st century AD) have been investigated (Del Vais 2018, 2010).

Underwater archaeological research in the lagoon has revealed the presence of important ancient contexts dating mainly from the Punic/Roman Republican period (7th–2nd century BC), with the sporadic attestation of artefacts from the Final Bronze age (10th century BC) and the Imperial Roman period (2nd century AD). The underwater archaeological site is located in the northern sector of the lagoon, in an area of ~210,000 m^2 (350 × 600 m); it is ~200 m from the north-east shore and extends south-westwards to ~800 m from the shore. Systematic surveys identified a widespread presence over the entire area of artefacts datable between the 6th and the 5th century BC, more rarely later. In a more limited sector (~5500 m^2), a high concentration of accumulated archaeological material was found, dating mainly from the 3rd–2nd century BC; in this sector, the underwater stratigraphic excavation was carried out in an area of ~120 square metres. The underwater research recovered abundant pottery, mostly transport amphorae, but also ceramics of domestic use and, more rarely, of a funerary and cultic nature (6th–3rd/2nd century BC). In several cases, the amphorae contained remains of animal bones, mostly of sheep and goats, showing clear evidence of slaughter processes. The silty substrate favoured the conservation of organic materials, including pinecones, seeds of different species (often contained also in the amphorae) and woods fragments (Del Vais et al. 2023a; Sabato et al. 2019; Del Vais and Sanna 2012). Among the numerous wooden artefacts lying under the amphorae deposit, horizontal elements were found joined to other vertical piles sinking on the sediment, which can be interpreted as possible structural parts of wooden jetties.

3 | Materials and Methods

3.1 | Geophysical Data

A grid of high-resolution seismic reflection lines with a total length of ~24 km was collected using a Chirp Benthos-Teledyne III system operating at a frequency of 2.5–7 kHz within the SGL (Figure 1) on board a small boat. The seismic lines were spaced approximately 200 m apart. The conversion of two-way travel time to approximate depth was obtained, assuming an average velocity of 1500 ms^{-1} in the water column and the saturated sediments of the first few metres below the lagoon bottom. The seismic reflection data provided a lateral resolution of 0.5 m and a vertical resolution of 0.25 m. The data were then processed and interpreted using Geosuite™ software, under the seismic stratigraphy paradigm (Mitchum et al. 1977).

Two geoelectric profiles were also carried out on the north-eastern shore of the lagoon (Figure 1). The survey consists of

measurements of the apparent resistivity of the ground using a quadrupole (four electrodes). Each measurement consists of injecting an electric current into the ground between two electrodes and measuring the voltage (potential difference) between the other two. We use a Wenner–Schlumberger acquisition scheme with 62 electrodes equally spaced at 1 m. This type of acquisition scheme is a good compromise between lateral and depth resolution. The data were then analysed to improve the signal-to-noise ratio by eliminating outliers and further inverted with a robust (L1-norm based) least square cost function to obtain two sections of the electrical resistivity of the subsoil (Figure 5). The 2-D inversion is justified by the flat geometry of the target bodies. However, it should be noted that the resistivity measurements can also be affected by structures off the profile lines.

3.2 | Coring and Sediment Analysis

A detailed knowledge of the stratigraphy of the River Tirso alluvial plain was available after the study of sediment cores reported in Figure 1 by De Falco et al. (2022) and Melis et al. (2017). In this study, six new sediment cores were collected along the north-eastern shore of the SGL and two sediment cores were collected from the lagoon bottom (Figure 1).

The cores collected from the lagoon shore reached depths of up to 10 m and covered the entire Holocene stratigraphic sequence overlying the Pleistocene alluvial sediments. Elevations of the cores relative to current mean sea level were obtained using a DGPS-RTK survey (vertical approximation ± 0.15 m).

Cores from the bottom of the lagoon were collected using a 1.2 m long PVC pipe manually pushed into the sediments. They were collected in two phases during the underwater archaeological excavations: directly on the lagoon floor and from sediments collected 1 m below the bottom, both in the same location. In this way, it was possible to recover a total of 2 m of sediment cores below the lagoon floor.

All cores were described for a preliminary lithofacies classification in the laboratory. Two cores (PT13bis, 11.4 m long, and C03, 2 m long) were sampled and analysed in more detail. The PT13bis and C03 cores were sampled at 10 and 5 cm intervals, respectively.

Each core interval was analysed for sediment grain size. Samples were wet-sieved at 90 μm, after pretreatment with H_2O_2, to separate the finer and coarser fractions. The former was analysed using a Galai CIS1 laser system and the latter by dry sieving (De Falco et al. 2015). The muddy layers of the cores contained several shell layers that were sampled. Additional shells were sampled during the grain size analysis. In addition, the muddy layers were analysed for water content and total organic matter by loss on ignition at 110° (12 h) and 550° (3 h), respectively.

X-ray fluorescence chemical analysis was carried out using an Olympus Vanta Element portable analyser (hereafter pXRF). The Vanta Element uses a 4 W/8–35 keV X-ray tube as an excitation source and a Si PIN as a detector. The XRF acquisition was carried out for the same core sampling interval along the exposed core section, with the sensor at a constant distance of 0.5 cm and an acquisition time of 120 s. The following elements, detected by XRF analysis, were selected: Sr, Pb, Zn and Mn. Pb, Zn and Mn are considered to be proxies for human activities, whereas Sr is a proxy for biogenic carbonate content in sediments (Simeone et al. 2022). The pXRF instruments yields the error (1σ) associated with the measure: 2% for Sr, 6% for Mn and 10% for Pb and Zn.

Malacological remains collected and sieved from the sampled sediments were analysed to define the palaeoecological conditions of the depositional environments. A first taxonomic identification was followed by a taphonomic analysis of shell condition and traces (fragmentation, internal biofouling and bioerosion marks, marine erosion, predation bores) (Claassen 1998; Poppe and Goto 1991, 1993; Doneddu and Trainito 2005). The ecological study of the different taphocoenoses has highlighted the biofacies, thereby refining our understanding of the ecological characteristics associated with each lithofacies.

3.3 | Core Dating

Five samples from the PT13bis core were collected for AMS ^{14}C radiocarbon dating, carried out at the of Beta Analytic's laboratories. Three samples of the mollusc *Cerastoderma glaucum* were found in life position with both articulated valves; two samples consisted of plant remains and sedimentary organic matter (Table 1).

Radiocarbon dates were calibrated using CALIB 8.2 (Stuiver et al. 2022). IntCal20 and Marine20 calibration methods were used. Local deviations of the marine reservoir effect were accounted for using a ΔR value of -137 ± 82, which is an average of the value for the area, including all available data for the westernmost part of the Mediterranean Sea (Heaton et al. 2020).

4 | Results

4.1 | Geophysical Data

The seismic reflection images allowed us to identify two seismic units (U1 and U2) overlying an acoustically blind unit (AcB). The seismic units are separated by two unconformities, which we have named S1 (the deeper one) and S2 (see Figure 2 for location; Figures 3 and 4).

The deeper units (U1 and AcB) and the stratigraphic surfaces S1 and S2 are not visible in continuity along the seismic sections due to the presence of gas and early diagenetic indurated facies in the sediments that were not penetrated by the acoustic signal. This made it difficult to correlate U1 throughout the study area. Unconformity S1 is located at variable depths, between approximately 6 and 14 m bpsl, in line with SG110 (Figure 4). S1 has the morphology of a large channel incision, approximately 1 km wide.

Unit U2 is characterised by sub horizontal parallel reflectors of low amplitude, onlapping S2, which has a roughly flat shape. The bottom of the lagoon is flat, with an average depth of about 1 m, tapering gently along the shoreline (Figures 3 and 4).

The resistivity tomography sections obtained on the northeastern shore of the lagoon are shown in Figure 5. In both cases, we

found a rapid increase in resistivity with extremely low values at shallow levels. The high conductivity in the upper layer makes it difficult to reach great depths. However, in both cases, there is a rapid increase in resistivity at around 6–8 m, indicating the presence of coarse Pleistocene sediments below this depth. The low resistivity in the upper layer is associated with silty–clayey deposits. It is interesting to note the presence of well-resolved lateral variations in the top layer, suggesting an alternance of layers with a different clay content.

4.2 | Core Data

The stratigraphic log of three cores drilled on the northeastern shore of the lagoon near the Sa Mitza channel (Figure 2) is shown in Figure 6; PT13bis was sampled and analysed in detail, whereas cores PT14 and PT15 were only described.

PT13bis was drilled down to a depth of 11.4 m, and the borehole was located at an elevation of 0.84 m above sea level. The first 0.64 m of the core consists of material of anthropic origin. The depths of the core logs, reported in Figure 6, are referenced to the elevation below the present sea level (depth bpsl).

The lowest part of the core (7.66–10.56 m bpsl) consists of rounded heterometric pebbles of different lithologies in a sandy matrix (Unit PL, Figure 6). The overlying Unit C4 (6.37–7.66 m bpsl) is a dark/black organic sandy mud with up to ~34% organic matter, rich in algal remains. The C4 unit was recovered discontinuously, and only three samples were collected and analysed. For each level, the sortable/non-sortable ratio (S/NS according to Mccave and Hall 2006) along the core was calculated. The S/NS ratio is the ratio between two grain size fractions (the sortable fraction corresponds to 8–63 μm and the non-sortable fraction is < 8 μm) and is a proxy of the hydrodynamic energy of the depositional environment. Along the C4 unit, the S/NS ratio is 0.4–1.6. The organic sediments from a layer at 7.56 m bpsl have been dated at 7375 ± 53 cal y BP (Table 1).

Unit C3 (3.83–6.36 m bpsl) consists of a greenish/grey mud interval rich in mica, with an organic matter content ranging from ~3% to ~6% (Figure 6). The S/NS ratio increases from 1.3 to 6. The C3 unit is characterised by the presence of shell fragments, generally bivalves, at various levels. However, shells with articulated valves were not found.

Unit C3 passes upward (3.83 m bpsl) to a 0.4 m thick layer composed of bioclastic muddy sandy gravels with abundant valves and fragments of *Cerastoderma glaucum* (typical of brackish ecosystems) and *Scrobicularia plana* (an intertidal species typical of transitional waters such as estuaries and very sheltered bays) dominating the taphocoenosis, both the species attesting to the formation of a typical lagoon. A valve of *C. glaucum* from a layer at 3.46 m bpsl was dated to 5049 ± 250 cal y BP (Table 1).

The uppermost unit C0 (0–3.26 m) consists of a dark grey sandy mud, with ~7%–8% organic matter. The deeper level of C0 contains a shell layer (2.63–3.26 m bpsl) with fossils of *S. plana* and *C. glaucum* in a silt/clay matrix, with several specimens in living position. A valve of *C. glaucum* from a layer at 2.76 m bpsl was dated to 4593 ± 244 cal y BP (Table 1). Upward along the

TABLE 1 | AMS ^{14}C radiocarbon age dating of shells and organic samples along the PT13bis core.

Core	Depth in core (m)	Elevation b.p.s.l. (m)	Sample description	^{14}C years BP	δ^{13}C	Calibration data set	Cal. age (2σ) years BP
PT13bis	1.9	1.1	Plant material	130 ± 30	−24.7	IntCal20	80 ± 72
PT13bis	2.4	1.6	*Cerastoderma glaucum*	700 ± 68	−6.4	Mixed marine/NoHem (74% Marine)	402 ± 145
PT13bis	3.6	2.8	*C. glaucum*	4420 ± 83	−1.5	Mixed marine/NoHem (94% Marine)	4593 ± 244
PT13bis	4.3	3.5	*C. glaucum*	4790 ± 87	−0.3	Marine20	5049 ± 250
PT13bis	7.4	6.6	Organic sediment	6470 ± 30	−25.5	IntCal20	7375 ± 53

Note: The radiocarbon ages were calibrated using CALIB 8.2 (Stuiver et al. 2022).

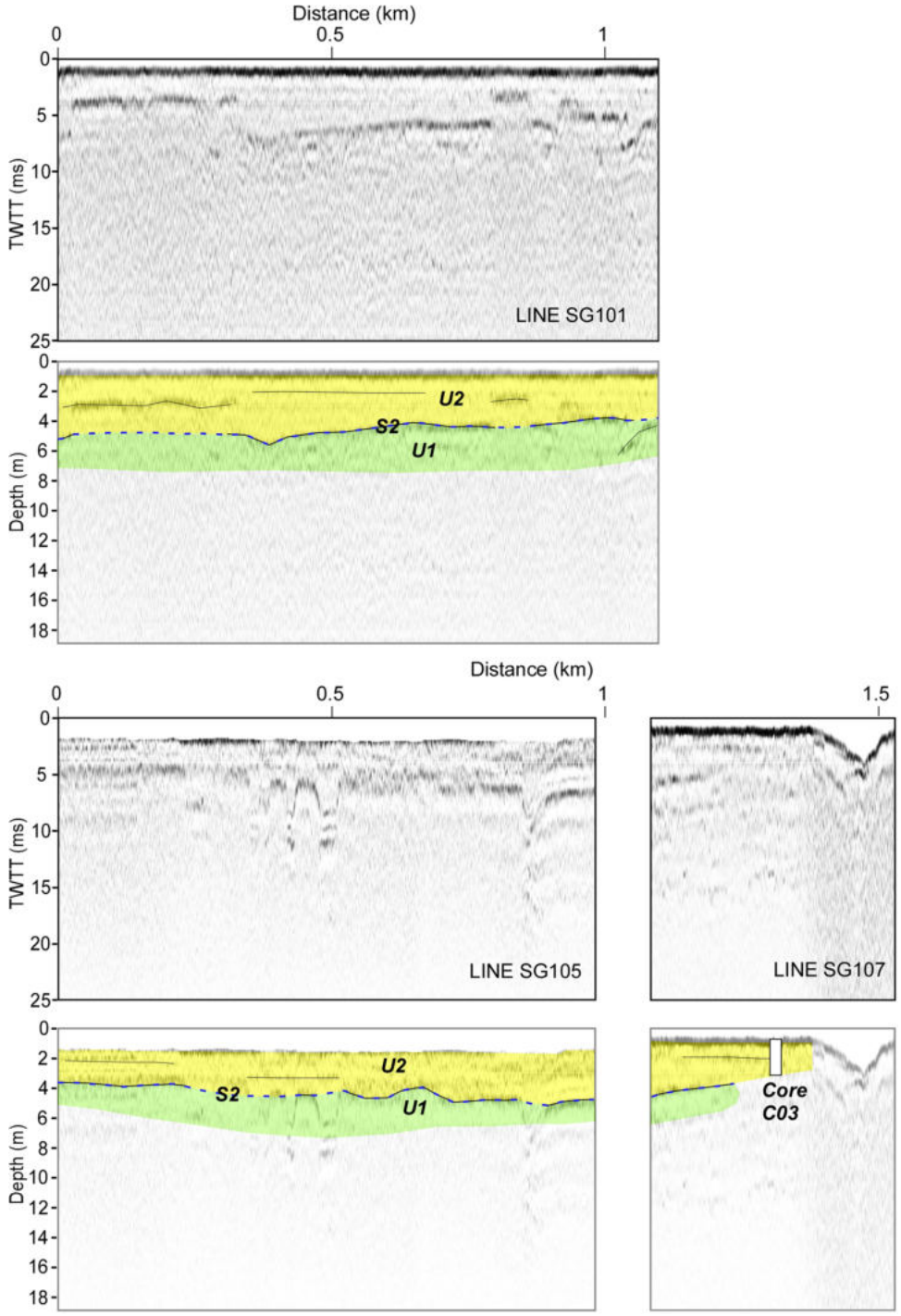

FIGURE 3 | Interpreted chirp sub-bottom seismic profiles collected in the Santa Giusta lagoon. The position of core C03 over line SG107 was reported. See Figure 2 of the seismic line position.

core, unit C0 is characterised by layers of *C. glaucum* in living position. A layer rich in organic matter (~10%–18%) was found at 0.96–1.26 m bpsl. The sortable/non sortable ratio increases from ~0.6 at the bottom to ~4 at the top of C0 (Figure 6). Two layers were dated (Table 1); these include a shell of *C. glaucum* sampled at 1.56 m bpsl, dated at 402 ± 145 cal y BP, and plant remains at 1.06 m, dated at 80 ± 72 cal y BP.

Cores PT15 and PT14 were drilled to depths of 10.5 and 12.7 m, respectively, at an elevation of 1.7 and 1.8 m. The first 1.6 m of both cores consisted of material of anthropic origin. The lowest part of both cores (down to ~2 m bpsl) consisted of reddish gravelly muddy sands and ochraceous mud (unit PL, Figure 6). Along core PT15, unit PL is overlain by grey coarse sands and muddy sands (unit B) and grey to greenish mud without bioclastic remains. Along core PT14, the unit PL is overlain by dark grey organic mud and sandy mud (unit C0) with specimens of *C. glaucum* and *S. plana*. Fragments of pottery and a piece of a kiln brick of Punic–Roman age were found at 0.2–0.6 m bpsl.

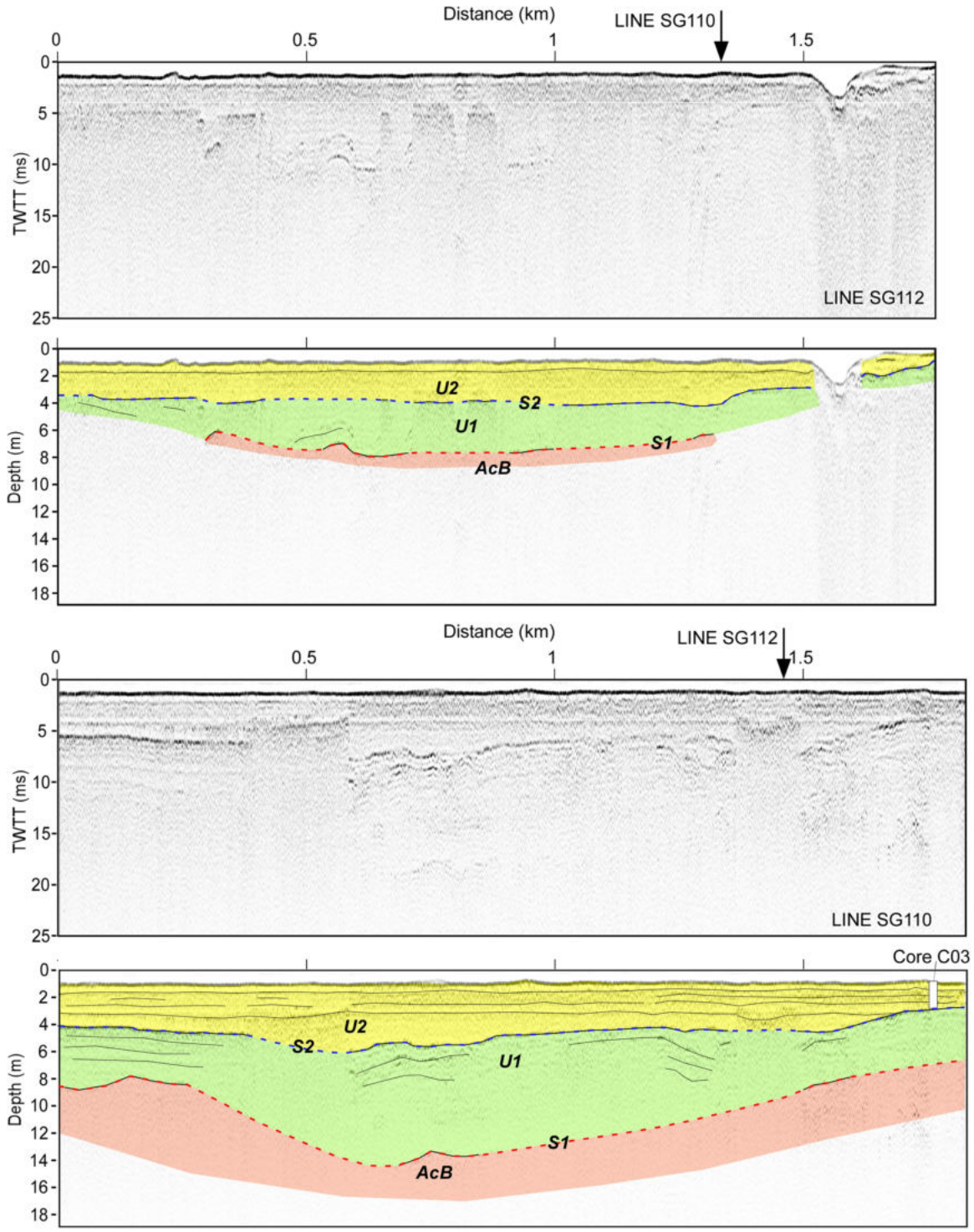

FIGURE 4 | Interpreted chirp sub-bottom seismic profiles collected in the Santa Giusta lagoon. The position of core C03 over line SG117 was reported. The morphology of the incised valley is visible in the line SG110. See Figure 2 of the seismic line position.

Concentrations of Sr, Pb, Zn and Mn along the PT13bis core, as determined by XRF analysis, are shown in Figure 7. They are slightly variable in the core intervals down to 3.7 m bpsl, corresponding to units C4 and C3. The concentration values range between 0.104 and 0.177 mg g^{-1} for Sr, between 0.014 and 0.03 mg g^{-1} for Pb, between 0.062 and 0.083 mg g^{-1} for Zn and between 0.325 and 0.463 mg g^{-1} for Mn (Figure 7). The Sr peak (0.342 mg g^{-1}) at 3 m bpsl corresponds to the level of bioclastic sands and gravels.

The upper part of the core, corresponding to the unit C0, is characterised by an increase in Pb, Zn and Mn (Figure 7). The peak concentration in Pb (0.05 mg g^{-1}) and Mn (1.193 mg g^{-1}) at one metre of depth bpsl corresponds to the level enriched in organic matter (Figures 6 and 7).

Core C03 (Figure 8) was taken inside the lagoon at 1 m depth. It is 2 m long and thus reaches 3 m bpsl. The sediments sampled are silty/clayey, with shelly layers present at 1.4 and 2.2 m bpsl,

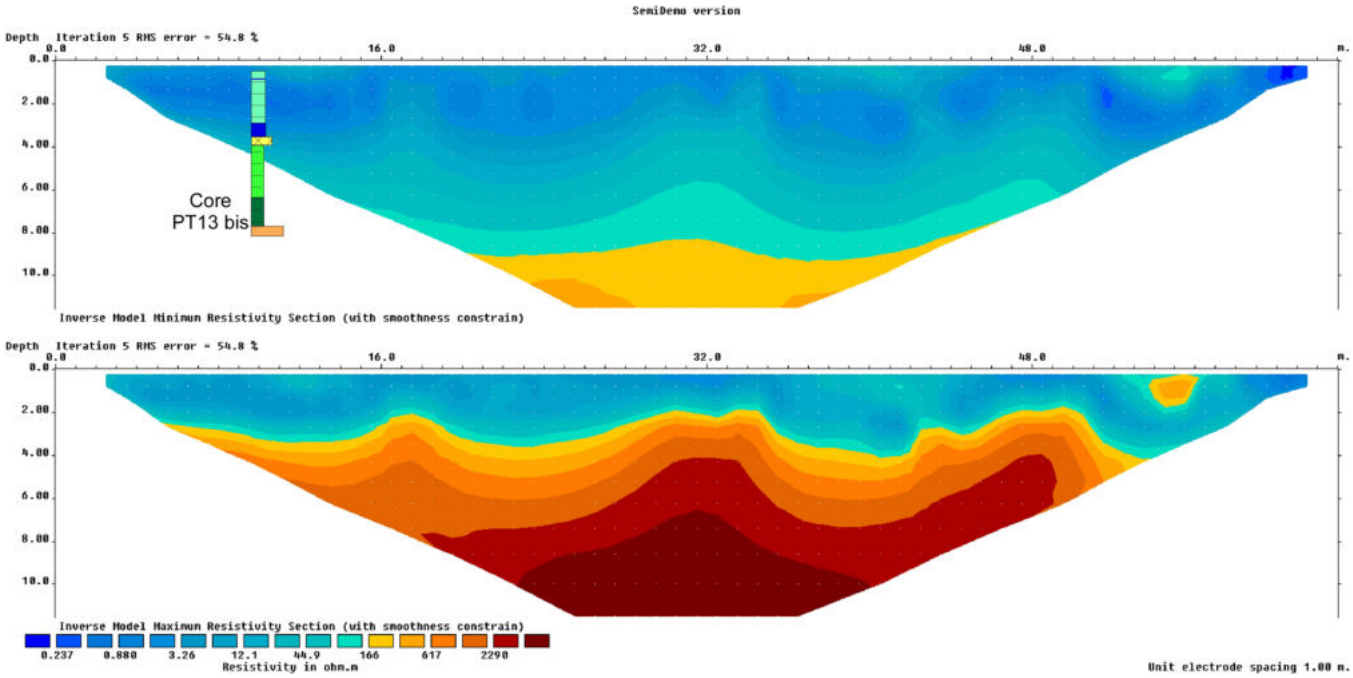

FIGURE 5 | Two resistivity tomography sections acquired along a transect crossing the core PT13 bis (see Figure 2). We registered a significant increase of resistivity with depth and lateral variations in the top level.

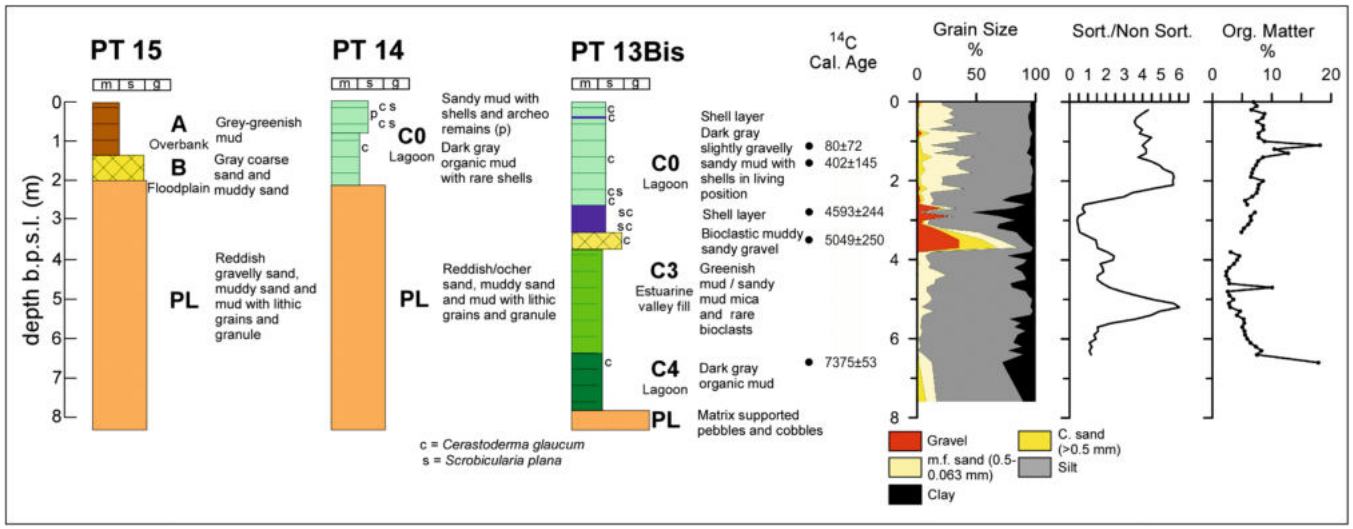

FIGURE 6 | Description and analysis of the cores PT13bis, PT14 and PT15 (see Figure 2 for borehole positions). For each log, the depth below the present sea level is provided. Sediment sections from the cores PT13bis were sampled and analysed for grain size, organic matter content, and faunal associations.

composed mainly of *C. glaucum*. The S/NS ratio is < 1. The Pb and Mn concentrations in the sediments are 0.03–0.15 and 0.41–1.13 mg g^{-1}, respectively (Figure 8).

5 | Discussion

5.1 | Depositional Environments and Stratigraphic Correlation

The reconstruction of the depositional environments and the stratigraphic correlation between the SGL and the River Tirso plain are shown in Figure 9. Cores PT8 and PT6 were collected along the Tirso River plain and were described in detail in a previous study (De Falco et al. 2022).

The PL unit of the core PT13bis can be interpreted as late Pleistocene alluvial coarse sediments that were incised by the River Tirso and its lateral tributaries during the last phase of sea-level lowstand (De Falco et al. 2022). The PL unit can be related to the acoustic basement traced in the seismic reflection profiles (AcB in Figure 4). The stratigraphic surface separating the PL unit from the overlying Holocene deposits can be interpreted as a subaerial unconformity (SU) (surface S1 in the seismic profiles, Figure 4).

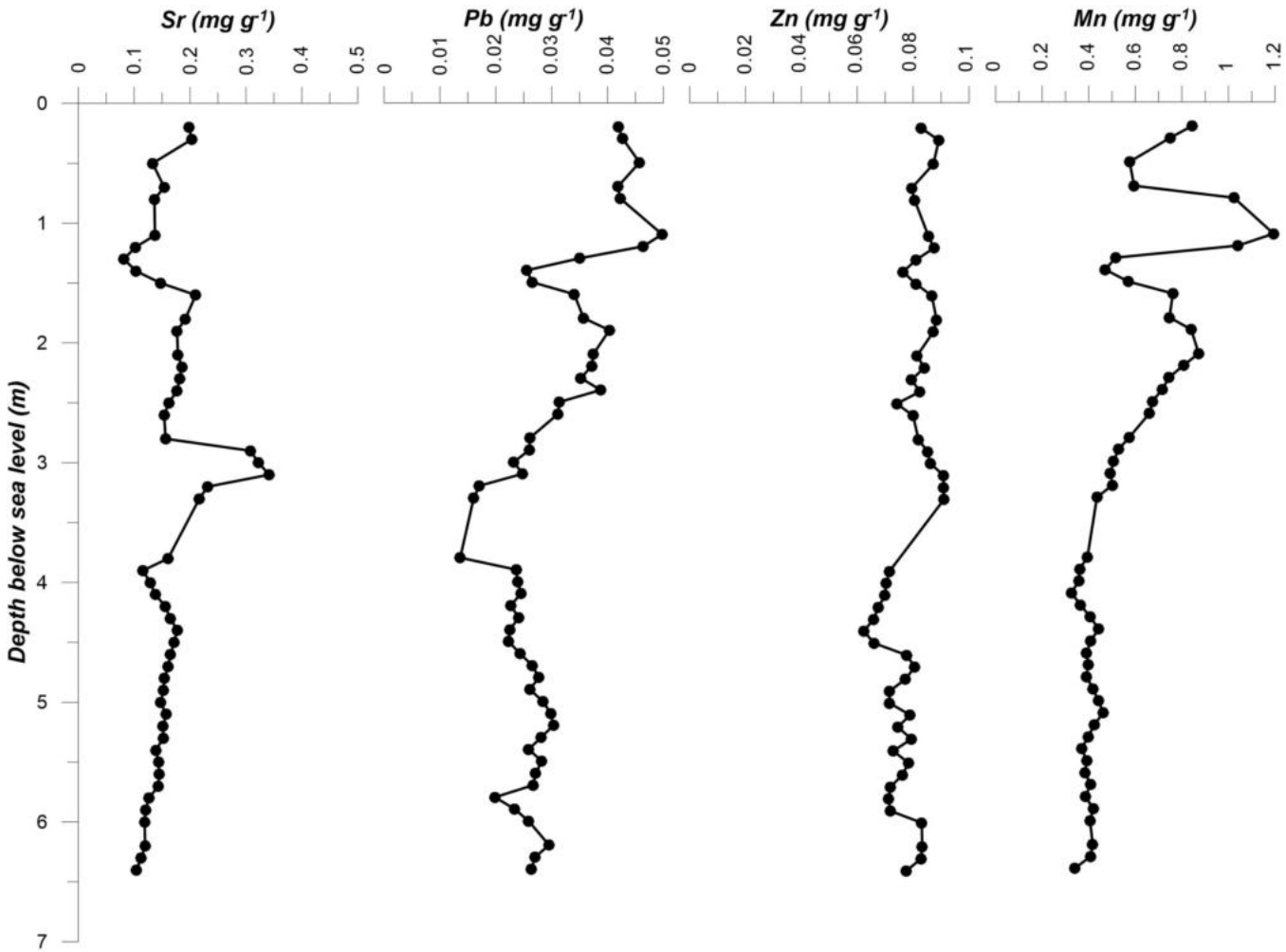

FIGURE 7 | Concentrations of Sr, Pb, Zn and Mn, along the PT13bis core profile measured by pXRF. The plots show the trend of an increase of metal (Pb, Zn and Mn) concentrations towards the top of the core. The peak of the Sr concentration at 3 m is related to a shell layer.

The morphology of this SU can be traced back to the formation of the incised valleys. In the resistivity profile shown in Figure 5, the Pleistocene deposits are characterised by a sharp increase in resistivity with depth, whereas the overlying silty–clay deposits are characterised by low resistivity values. The overlying units C4 and C3 in core PT13bis may be correlated with unit C3 in cores PT6 and PT8. In both sediment cores, C3 consists of terrigenous muddy sediments with abundant mica and bioclast fragments (De Falco et al. 2022). The sedimentation environment was probably an estuary with a rapid sedimentation rate. Based on available radiocarbon data, sedimentation rates of C3 are estimated at 1.3 ± 0.2 mm year^{-1} in core PT13 Bis and 4.7 ± 0.7 mm year^{-1} in core PT8. Units C4 and C3 can be correlated with the U1 unit in seismic sections (Figures 3, 4, and 9).

A level of coarse sediment dated at ~5 ka marks the transition to the overlying C0 unit of core PT13bis, which correlates with C2 and C0 of cores PT8 and PT9. Unit C0 can be attributed to a lagoonal environment due to the presence of fauna of transitional environments (*C. glaucum* and *S. plana*), with shells in life position. Unit C0 is characterised by a reduced sedimentation rate down to 0.3 ± 0.05 mm year^{-1}. A level of coarse sediments in core PT13bis, which marks the transition to the overlying C0 unit, can be correlated to surface S2 in seismic sections and the overlying C0 unit to unit U2. The U2 seismic unit was sampled within the lagoon by core C03. The sediments of the C03 core are silt/clayey, with shelly beds composed mainly of *C. glaucum*. The sediments of core C03 show the same sedimentological character and faunal content as the C0 unit of core PT13bis. The establishment of a lagoon environment, both in the river plan of the Tirso and in the SGL, can be related to the formation of coastal barriers that partially closed the depressions occupied by the incised valleys from ~6 ka, in response to the progradation of the coastal systems after sea level stabilised (Giaime et al. 2019; Anthony et al. 2014; Catuneanu and Zecchin 2013).

Subsequently, at 4.5 ka, fluvial levee, channel and overbank sediments were deposited along the river plain, as recorded in the upper part of cores PT8 and PT6 (Figure 9) (De Falco et al. 2022; Melis et al. 2017). After 4.5 ka, the SGL had been partially filled by lagoon sediments containing archaeological deposits, at an elevation of 2 m bpsl. The excavated archaeological materials lie upon and above a Cerastoderma layer (suggesting a phase of minor sedimentary supply) and embedded in the fine sediments (dark grey sandy mud) of the lagoon. The age of the archaeological deposits is mainly Punic/Republican Roman (2.6–2.1 ka), although some Imperial

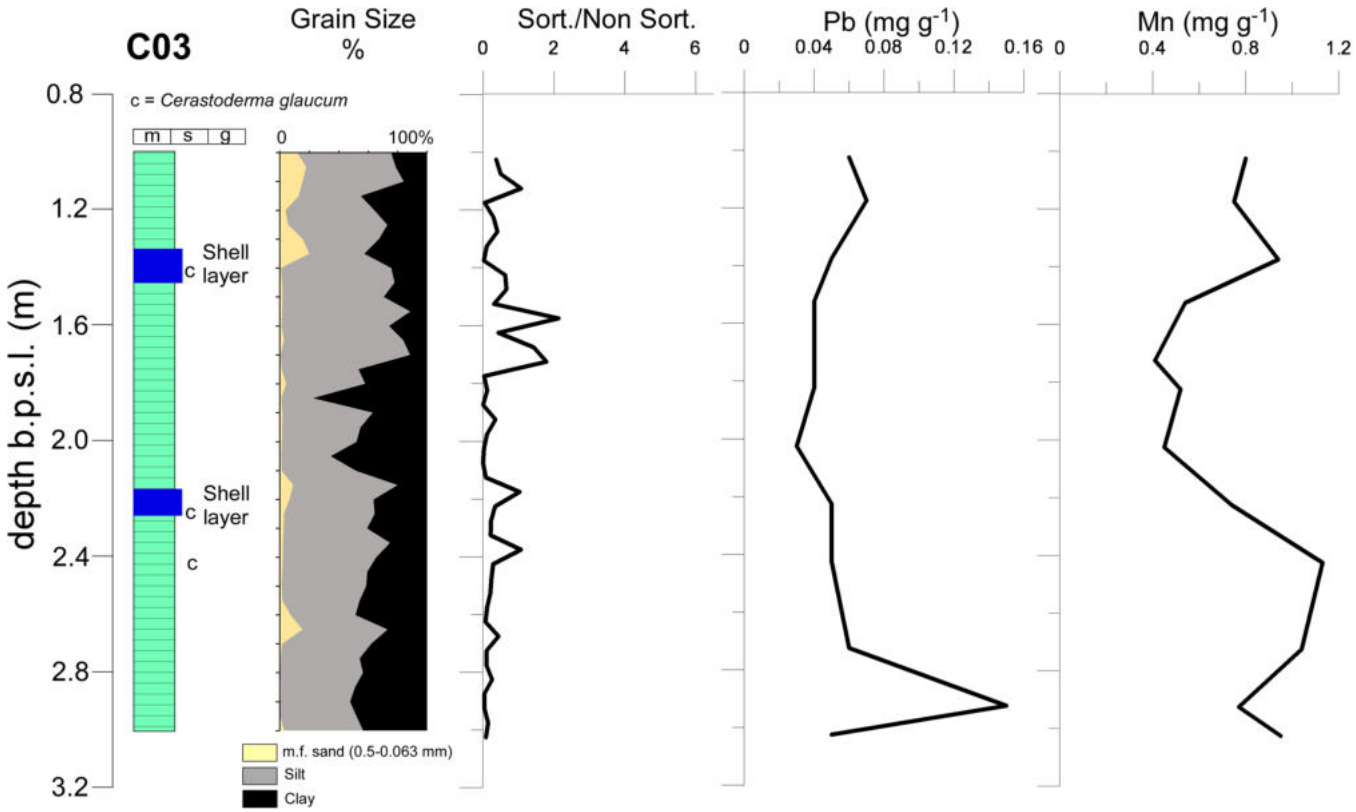

FIGURE 8 | Grain size and XRF data measured along the sediment core C03 collected inside the lagoon (see Figure 2 for the sampling point position).

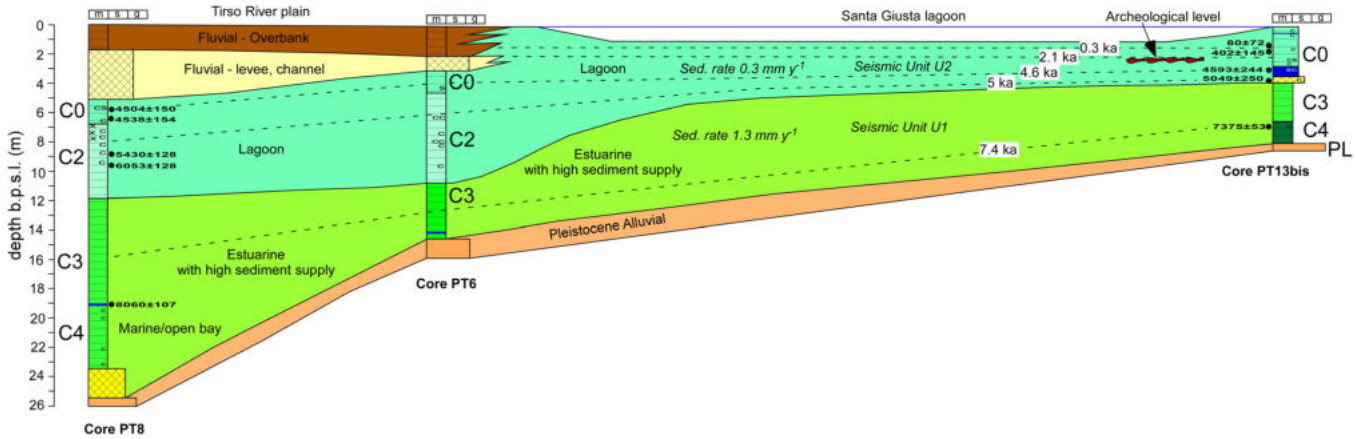

FIGURE 9 | Stratigraphic correlations among the core PT13bis (this study), PT6 and PT8 (De Falco et al. 2022) The interpretations of sedimentation environments, seismic units and seismic surfaces were also reported.

Roman amphorae are present, extending the dating of the deposit to 1.8 ka (Figure 9).

The error associated with the radiocarbon dating of the proxies used for chronostratigraphic reconstruction is < 0.25 ka (Table 1). This error does not significantly affect the reconstruction of depositional environments based on chronostratigraphic analysis of sediment cores. The shells of *C. glaucum* used for dating had articulated valves and were encountered in their likely living position. Core PT13bis, on which the chronostratigraphic reconstruction was based, was taken at the edge of the lagoon, in an area unaffected by the dredging carried out inside the lagoon. Therefore, the stratigraphic record of core PT13bis shows no evidence of erosion or discontinuous lack of sedimentation as a result of dredging, and can be considered undisturbed.

5.2 | Palaeo-Environmental Evolution

Based on stratigraphic and archaeological data, we can reconstruct the palaeoenvironmental evolution of the SGL site from ~7.5 ka (Figure 10). The morphology of the SU, reconstructed from seismic reflection profiles and core stratigraphy, indicates that the lagoon is

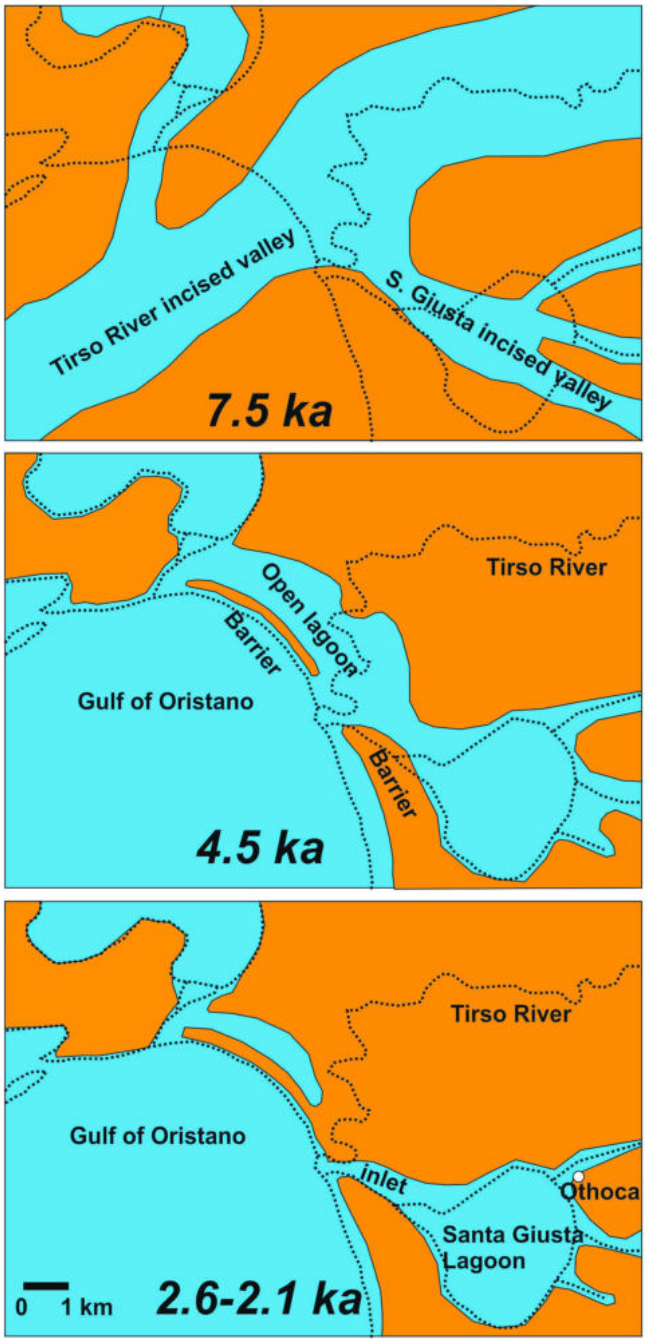

FIGURE 10 | Sketch showing the reconstruction of the geomorphological evolution of the Santa Giusta lagoon and Tirso River mouth since 7.5 ka, based on this study (Santa Giusta lagoon), Melis et al. (2017) (right riverbank) and De Falco et al. (2022) (Tirso River mouth).

the result of the flooding of the incised valley of a tributary of the Tirso River as a consequence of the post-LGM sea-level rise (Figure 10). The maximum depth of the incised valley below the SGL can be estimated at 14 m bpsl (Figure 4). According to the curves available for the study area (De Falco et al. 2022; Vacchi et al. 2016), the sea level reached the height of 14 m bpsl at ~8 ka, progressively flooding the incised valley and minor tributaries. During the valley flooding phase, between ~8 ka and ~5–6 ka, the depositional environment was an estuary with a sedimentation rate of about 1.3 ± 0.2 mm year^{-1}. Silty–clayey sediments partially filled the palaeo-valley. During this period, the rate of sea-level rise decreased from ~6 to ~2 mm year^{-1} (Vacchi et al. 2021), a value higher than the sedimentation rate estimated for the estuarine deposits, indicating overaccommodation.

Between ~6 and ~4.5 ka, the deposition of fine-grained lagoon sediments in the alluvial plain suggests the effect of coastal barriers protecting the environment from the high-energy sedimentary processes typical of the coastal environment. In this phase, the incised valley of Santa Giusta is characterised by the presence of a lagoon environment, which is connected to the mouth of the River Tirso. The observations led to the compilation of the palaeoenvironmental reconstruction synthetised in Figure 10, which suggests that a large open lagoon occupied the coastal area at 7.5 ka and was subsequently separated from the sea by a system of coastal barriers from 6 ka, in agreement with the reconstruction proposed by De Falco et al. (2022) and Melis et al. (2017). After this phase, alluvial sediments were deposited on the plain of the River Tirso, resulting in the progressive isolation of the SGL. Evidence of anthropic occupation of the site since ~4.5 ka is provided by the increase in Pb, Mn and Zn concentrations in the sedimentary record (Figure 7).

Radiocarbon data from sediment core PT13bis highlight that, starting from 4.5 ka, the sedimentation rate within the SGL reduced to 0.3 ± 0.05 mm year^{-1}. Sea-level curves for the study area indicate that around 2 ka, sea level was approximately at the present level (Vacchi et al. 2016; Pascucci et al. 2018; De Falco et al. 2022), although other authors indicate a sea level of about 1.8 m below the present level for the same period (Antonioli et al. 2007). Considering a palaeo sea level similar to the present between 2.6 and 1.8 ka, we can estimate a lagoon depth of 1.5–1.8 m based on the height of the archaeological level.

The underwater archaeological context is embedded in the lagoon sediments, corresponding to unit C0 and seismic unit U2, which comprise three archaeological sub-layers. The presence of numerous transport amphorae and wooden structures indicates a possible maritime activity in a natural harbour, such as the inundated space of the lagoon of Santa Giusta accessible through inlets during the Punic period (since ~2.6 ka). The recent re-examination of stratigraphic sequences and archaeological material indicates an extension of the period of occasional frequentation of the natural harbour to the Roman Imperial period (2nd century AD) (~2.1–1.8 ka), probably with vessels of medium tonnage and shallow draught for shallow waters, such as Punic trading ships or Roman transhipment vessels (de Juan Fuertes 2017; Medas 2000). The amphorae and other Punic archaeological remains were located at a shallow depth; various markers formed on the lagoon floor were observed on their surfaces: patinas of microalgae biofilms, abrasions, carbonate concretions and attacks by lignivorous organisms (*Teredo navalis*). This suggests an initial underwater phase with microalgae colonisation, which was short-lived, given the limited presence of carbonate concretions from aquatic worms and lignivorous aggression on wooden artefacts, which would have been interrupted by the sedimentary cover of anoxic mud (Del Vais and Sanna 2012). After 2.1–1.8 ka, there is little evidence of the use of SGL as a lagoon harbour in Roman Imperial time. The abandonment of the site as a lagoonal harbour is probably not due to silting, given the low sedimentation

rate (0.3 ± 0.5 mm year^{-1}), but due to the narrowing of the lagoon mouth. Indeed, the accelerated progradation of the Tirso River mouth, which can be estimated at 0.5 km ka^{-1}, is likely to have resulted in excessive narrowing of the lagoon inlets, thus leading to a progressive abandonment of the site as a navigable area.

The stratigraphic data demonstrate a transition between estuarine and lagoonal environments, which can be attributed to the formation of coastal barriers and subsequent progradation of the river mouth. The age of this transition is consistent with elevated progradation rates affecting Mediterranean coasts, which followed a major reduction in the rate of sea-level rise at around 6 ka (Amorosi et al. 2017; Vacchi et al. 2016; Anthony et al. 2014). Therefore, the evolution of the SGL site is consistent with models proposed for other coeval coastal sites in eastern Sardinia (Melis et al. 2018) and Corsica (Currás et al. 2017; Ghilardi et al. 2017; Vacchi et al. 2017).

6 | Conclusion

The human occupation of the natural lagoon harbour of Santa Giusta was strictly conditioned by the progradation of the alluvial system of a major river in the western Sardinia, the Tirso. Several lines of evidence suggest that the Santa Giusta lagoon is the result of the flooding and infilling of an incised valley formed by a tributary of the River Tirso. Around 6 ka, coastal processes dominated the sedimentary infilling of the incised valley, following a slowdown in the rate of sea-level rise. The development of coastal barriers led to the formation of a large open lagoon, occupying the entire present area of the river mouth. From 4.5 ka, the river alluvial system advanced towards the river mouth, with the deposition of levee and overbank fluvial deposits. This sedimentation has progressively isolated the Santa Giusta lagoon and reduced the size of the inlets. Archaeological evidence shows that the lagoon, including the access channels, was still navigable in the Punic/Roman Republican period. The progressive abandonment of the site as lagoonal harbour, which took place during the Roman Imperial period, is probably linked to the progressive narrowing of the inlets, which were reduced to small channels accessible only to small boats.

Acknowledgements

We acknowledge G. Stanghellini (CNR ISMAR Bologna) for the support for the seismic survey, Francesco Basile and Giuseppe Della Monica (Roma Tre University) for the support in geoelectric acquisition, Lucia Simone and Gabriele Carannante (University of Naples "Federico II") for support in processing palaeoecological data and Sietske Batenburg for the revision of English text. The work has been funded by grant Legge Regionale 7/2007 Project: "Interazioni tra uomo e ambiente nell'evoluzione del paesaggio costiero antico della Sardegna," funded by Regione Autonoma della Sardegna (RAS), Assessorato della Programmazione, Bilancio, Credito e Assetto del Territorio (Base Research Project, L.R. 7 agosto 2007, n. 7, Annualità 2013 (Resp. Carla Del Vais). Partial funding was provided by the projects RITMARE ICM Golfo di Oristano—Linea Dati (Reso. Giovanni De Falco), funded by the Italian Ministry of Research and Education and DESIRMED Demonstration and mainstreaming of Nature-based Solutions for Climate Resilient transformation in the Mediterranean, under the call HORIZON-MISS-2022-CLIMA-01-06, Grant Agreement No 101112972. Open access publishing facilitated by Consiglio Nazionale delle Ricerche, as part of the Wiley - CRUI-CARE agreement.

References

Acquaro, E., B. Marcolongo, F. Vangelista, and F. Verga eds. 1999. II Portto buono di Tharros. *Studi e ricerche sui Beni Culturali*.

Amorosi, A., L. Bruno, B. Campo, et al. 2017. "Global Sea-Level Control on Local Parasequence Architecture From the Holocene Record of the Po Plain, Italy." *Marine and Petroleum Geology* 87: 99–111. https://doi.org/10.1016/j.marpetgeo.2017.01.020.

Anthony, E. J., N. Marriner, and C. Morhange. 2014. "Human Influence and the Changing Geomorphology of Mediterranean Deltas and Coasts Over the Last 6000 Years: From Progradation to Destruction Phase?" *Earth-Science Reviews* 139: 336–361. https://doi.org/10.1016/j.earscirev.2014.10.003.

Antonioli, F., M. Anzidei, K. Lambeck, et al. 2007. "Sea-Level Change During the Holocene in Sardinia and in the Northeastern Adriatic (Central Mediterranean Sea) From Archaeological and Geomorphological Data." *Quaternary Science Reviews* 26: 2463–2486. https://doi.org/10.1016/j.quascirev.2007.06.022.

Bellotti, P., G. Calderoni, F. Di Rita, et al. 2011. "The Tiber River Delta Plain (Central Italy): Coastal Evolution and Implications for the Ancient Ostia Roman Settlement." *Holocene* 21: 1105–1116. https://doi.org/10.1177/0959683611400464.

Casula, G., A. Cherchi, L. Montadert, M. Murru, and E. Sarria. 2001. "The Cenozoic Graben System of Sardinia (Italy): Geodynamic Evolution From New Seismic and Field Data." *Marine and Petroleum Geology* 18: 863–888. https://doi.org/10.1016/S0264-8172(01)00023-X.

Cataudella, S., D. Crosetti, and F. Massa, eds. 2015. *Mediterranean Coastal Lagoons: Sustainable Management and Interactions Among Aquaculture, Capture Fisheries and the Environment*. General Fisheries Commission for the Mediterranean, Studies and Reviews 95, Rapport de la FAO.

Catuneanu, O., and M. Zecchin. 2013. "High-Resolution Sequence Stratigraphy of Clastic Shelves II: Controls on Sequence Development." *Marine and Petroleum Geology* 39, no. 1: 26–38. https://doi.org/10.1016/j.marpetgeo.2012.08.010.

Cherchi, A., N. Mancin, L. Montadert, et al. 2008. "The Stratigraphic Response to the Oligo-Miocene Extension in the Western Mediterranean From Observations on the Sardinia Graben System (Italy)." *Bulletin de la Société géologique de France* 179, no. 3: 267–287. https://doi.org/10.2113/gssgfbull.179.3.267.

Claassen, C. 1998. *Shells. Cambridge Manuals in Archaeology*. Cambridge University Press.

Cocco, F., S. Andreucci, D. Sechi, G. Cossu, and A. Funedda. 2019. "Upper Pleistocene Tectonics in Western Sardinia (Italy): Insights From the Sinis Peninsula Structural High." *Terranova* 31, no. 5: 485–493. https://doi.org/10.1111/ter.12418.

Currás, A., M. Ghilardi, K. Peche-Quilichini, et al. 2017. "Reconstructing Past Landscapes of the Eastern Plain of Corsica (NW Mediterranean) During the Last 6000 Years Based on Molluscan, Sedimentological and Palynological Analyses." *Journal of Archaeological Science: Reports* 12: 755–769. https://doi.org/10.1016/j.jasrep.2016.09.016.

De Falco, G., F. Antonioli, G. Fontolan, V. Lo Presti, S. Simeone, and R. Tonielli. 2015. "Early Cementation and Accommodation Space Dictate the Evolution of Barrier System During the Holocene." *Marine Geology* 369: 52–66. https://doi.org/10.1016/j.margeo.2015.08.002.

De Falco, G., A. Carannante, C. Del Vais, et al. 2022. "Evolution of a Single Incised Valley Related to Inherited Geology, Sea Level Rise and Climate Changes During the Holocene (Tirso River, Sardinia, Western

Mediterranean Sea)." *Marine Geology* 451: 106885. https://doi.org/10.1016/j.margeo.2022.106885.

De Juan Fuertes, J. 2017. "Técnicas de arquitectura naval de la cultura fenicia." *SPAL Revista de Prehistoria y Arqueología de la Universidad de Sevilla* 26: 59–85.

Del Vais, C. 2010. "L'abitato fenicio-punico e romano." In *La Cattedrale di Santa Giusta*, Architettura e arredi dall'XI al XIX secolo, edited by R. Coroneo, 35–46.

Del Vais, C. 2014. "Il Sinis di Cabras in età punica." In *Le sculture di Mont'e Prama*, edited by M. Minoja and A. Usai, 103–136. Contesto, scavi e materiali.

Del Vais, C. 2018. "Othoca in età punica: i dati delle fonti archeologiche." *Byrsa*, 33–34, 89–107.

Del Vais, C., A. Carannante, S. Chilardi, et al. 2023a. "Ricerche archeologiche subacquee e indagini geoarcheologiche per la definizione della portualità della città di Othoca." *Byrsa* 43: 91–112.

Del Vais, C., A. Carannante, S. Chilardi, et al. 2023b. "Per una ricostruzione del porto di Tharros: prospezioni, scavi archeologici costieri e indagini geoarcheologiche." *Byrsa* 43: 113–141.

Del Vais, C., A. Depalmas, A. C. Fariselli, R. T. Melis, and G. Pisanu. 2008. "Ricerche geoarcheologiche nella Penisola del Sinis (OR): aspetti e modificazioni del paesaggio tra preistoria e storia." In *Simposio Il monitoraggio costiero mediterraneo: problematiche e tecniche di misura (Napoli, 4–6 giugno 2008)*, edited by I. I. Atti del, 403–414. CNR-IBIMET.

Del Vais, C., V. Pascucci, G. De Falco, et al. 2020. "Scavi e ricerche geoarcheologiche e paleoambientali nell'area del porto di Tharros (laguna di Mistras, Cabras)." In *A Journey Between East and West in the Mediterranean. IX International Congress of Phoenician and Punic Studies*, edited by S. Celestino Pérez and E. Rodríguez González, 879–888. Instituto de Arqueología, Mérida (CSIC-Junta de Extremadura).

Del Vais, C., and I. Sanna. 2012. *Nuove ricerche subacquee nella laguna di Santa Giusta (OR) (campagna del 2009-2010)*. ArcheoArte. Rivista elettronica di Archeologia e Arte.

Doneddu, M., and E. Trainito. 2005. *Conchiglie del Mediterraneo*. Milano, Il Castello.

Ghilardi, M., D. Istria, A. Currás, et al. 2017. "Reconstructing the Landscape Evolution and the Human Occupation of the Lower Sagone River (Western Corsica, France) From the Bronze Age to the Medieval Period." *Journal of Archaeological Science: Reports* 12: 741–754. https://doi.org/10.1016/j.jasrep.2016.07.009.

Giaime, M., M. Artzy, H. M. Jol, Y. Salmon, G. I. López, and A. Abu Hamid. 2022. "Refining Late-Holocene Environmental Changes of the Akko Coastal Plain and Its Impacts on the Settlement and Anchorage Patterns of Tel Akko (Israel)." *Marine Geology* 447: 106778. https://doi.org/10.1016/j.margeo.2022.106778.

Giaime, M., N. Marriner, and C. Morhange. 2019. "Evolution of Ancient Harbours in Deltaic Contexts: A Geoarchaeological Typology." *Earth-Science Reviews* 191: 141–167. https://doi.org/10.1016/j.earscirev.2019.01.022.

Giaime, M., C. Morhange, M. Á. Cau Ontiveros, J. J. Fornós, M. Vacchi, and N. Marriner. 2017. "In Search of Pollentia's Southern Harbour: Geoarchaeological Evidence From the Bay of Alcúdia (Mallorca, Spain)." *Palaeogeography, Palaeoclimatology, Palaeoecology* 466: 184–201. https://doi.org/10.1016/j.palaeo.2016.11.023.

Heaton, T. J., P. Köhler, M. Butzin, et al. 2020. "Marine20—The Marine Radiocarbon Age Calibration Curve (0–55,000 cal BP)." *Radiocarbon* 62, no. 4: 779–820. https://doi.org/10.1017/RDC.2020.68.

IIPP. 2009. *Atti della XLIV Riunione scientifica dell'Istituto Italiano di Preistoria e Protostoria*. La preistoria e la protostoria della Sardegna (Cagliari, Barumini, Sassari, 23-28 novembre 2009), I, Relazioni generali, Firenze.

Kaniewski, D., N. Marriner, C. Morhange, et al. 2018. "Holocene Evolution of Portus Pisanus, the Lost Harbour of Pisa." *Scientific Reports* 8: 11625. https://doi.org/10.1038/s41598-018-29890-w.

Marriner, N., and C. Morhange. 2007. "Geoscience of Ancient Mediterranean Harbours." *Earth-Science Review* 80, no. 3–4: 137–194. https://doi.org/10.1016/j.earscirev.2006.10.003.

Maselli, V., and F. Trincardi. 2013. "Large-Scale Single Incised Valley From a Small Catchment Basin on the Western Adriatic Margin (Central Mediterranean Sea)." *Global and Planetary Change* 100: 245–262. https://doi.org/10.1016/j.gloplacha.2012.10.008.

Mccave, I. N., and I. R. Hall. 2006. "Size Sorting in Marine Muds: Processes, Pitfalls, and Prospects for Paleoflow-Speed Proxies." *Geochemistry, Geophysics, Geosystems* 7: Q10N05. https://doi.org/10.1029/2006GC001284.

Medas, S. 2000. *La marineria cartaginese, le navi, gli uomini, la navigazione*. Sardegna Archeologica. Scavi e Ricerche, 2, Carlo Delfino editore (Sassari).

Melis, R. T., A. Depalmas, F. Di Rita, F. Montisa, and M. Vacchi. 2017. "Mid to Late Holocene Environmental Changes Along the Coast of Western Sardinia (Mediterranean Sea)." *Global and Planetary Change* 155: 29–41. https://doi.org/10.1016/j.gloplacha.2017.06.001.

Melis, R. T., F. Di Rita, C. French, et al. 2018. "8000 Years of Coastal Changes on a Western Mediterranean Island: A Multiproxy Approach From the Posada Plain of Sardinia." *Marine Geology* 403: 93–108. https://doi.org/10.1016/j.margeo.2018.05.004.

Mitchum, J. R., P. R. Vail, and J. B. Sangree. 1977. "Stratigraphic Interpretation of Seismic Reflection Pattern in Depositional Sequences." In *Seismic Stratigraphy—Applications to Hydrocarbon Exploration,* AAPG Memoirs, edited by C. E. Payton, Vol. 26, 117–134. American Association of Petroleum Geologists. https://doi.org/10.1306/M26490C8.

Morhange, C., N. Marriner, G. Bony, C. Flaux, M. Giaime, and M. Kouka. 2017. "Geoarchaeology of Ancient Harbours in Lagoonal Contexts: An Introduction." In *Fluvial Landscapes in the Roman World, Journal of Roman Archaeology, supplementary series*, edited by T. Franconi, Vol. 104, 97–110.

Pascucci, V., G. De Falco, C. Del Vais, I. Sanna, R. T. Melis, and S. Andreucci. 2018. "Climate Changes and Human Impact on the Mistras Coastal Barrier System (W Sardinia, Italy)." *Marine Geology* 395: 271–284. https://doi.org/10.1016/j.margeo.2017.11.002.

Poppe, G. T., and Y. Goto. 1991. *European Seashells* (I). Christa Hemmen Verlag.

Poppe, G. T., and Y. Goto. 1993. *European Seashells* (II). Christa Hemmen Verlag.

Ruiz-Pérez, J. M., and P. Carmona. 2019. "Turia River Delta and Coastal Barrier-Lagoon of Valencia (Mediterranean Coast of Spain): Geomorphological Processes and Global Climate Fluctuations Since Iberian-Roman Times." *Quaternary Science Reviews* 219: 84–101. https://doi.org/10.1016/j.quascirev.2019.07.005.

Sabato, D., L. Peña-Chocarro, M. Ucchesu, et al. 2019. "New Insights About Economic Plants During the 6th-2nd Centuries BC in Sardinia, Italy." *Vegetation History and Archaeobotany* 28, no. 1: 9–16. https://doi.org/10.1007/s00334-018-0680-0.

Simeone, S., A. G. L. Palombo, F. Antognarelli, W. Brambilla, A. Conforti, and G. De Falco. 2022. "Sediment Budget Implications From *Posidonia oceanica* Banquette Removal in a Starved Beach System." *Water* 14, no. 15: 2411. https://doi.org/10.3390/w14152411.

Spanu, P. G., and R. Zucca. 2011. *Da Τάρραι πόλις al portus sancti Marci: storia e archeologia di una città portuale dall'antichità al Medioevo*. In Tharros Felix, Vol. 4, 15–103.

Stefaniuk, L., and C. Morhange. 2010. "Evoluzione dei paesaggi littorali nella depressione sudovest di Cuma da 4000 anni, il problema del porto antico." In *Atti del 40 convegno di studi sulla Magna Grecia, Taranto (2008)*, edited by A. Alessio, M. Lombardo, and A. Siciliano, 305–322. Istituto per la storia e l'archeologia della Magna Grecia.

Stuiver, M., P. J. Reimer, and R. W. Reimer. 2022. CALIB 8.2 (WWW program) at http://calib.org.

Usai, A., S. Sebis, A. Depalmas, et al. 2012. "L'insediamento nuragico di Sa Osa (Cabras-OR)." In *Atti della XLIV Riunione scientifica dell'Istituto Italiano di Preistoria e Protostoria. La preistoria e la protostoria della Sardegna (Cagliari, Barumini, Sassari, 23–28 novembre 2009)* II, edited by C. Lugliè, 771–782. Comunicazioni, Firenze.

Vacchi, M., M. Ghilardi, G. Spada, A. Currás, and S. Robresco. 2017. "New Insights Into the Sea-Level Evolution in Corsica (NW Mediterranean) Since the Late Neolithic." *Journal of Archaeological Science: Report* 12: 783–793. https://doi.org/10.1016/j.jasrep.2016.07.006.

Vacchi, M., K. M. Joyse, R. E. Kopp, N. Marriner, D. Kaniewski, and A. Rovere. 2021. "Climate Pacing of Millennial Sea-Level Change Variability in the Central and Western Mediterranean." *Nature Communications* 12: 4013. https://doi.org/10.1038/s41467-021-24250-1.

Vacchi, M., N. Marriner, C. Morhange, G. Spada, A. Fontana, and A. Rovere. 2016. "Multiproxy Assessment of Holocene Relative Sea-Level Changes in the Western Mediterranean: Sea-Level Variability and Improvements in the Definition of the Isostatic Signal." *Earth-Science Reviews* 155: 172–197. https://doi.org/10.1016/j.earscirev.2016.02.002.